

---

---

# Whole-Body Voxel-Based Personalized Dosimetry: The Multiple Voxel S-Value Approach for Heterogeneous Media with Nonuniform Activity Distributions

Min Sun Lee<sup>1,2</sup>, Joong Hyun Kim<sup>3</sup>, Jin Chul Paeng<sup>1</sup>, Keon Wook Kang<sup>1,4</sup>, Jae Min Jeong<sup>1,2,4</sup>, Dong Soo Lee<sup>1</sup>, and Jae Sung Lee<sup>1,2,4</sup>

<sup>1</sup>Department of Nuclear Medicine, College of Medicine, Seoul National University, Seoul, Korea; <sup>2</sup>Interdisciplinary Program in Radiation Applied Life Science, Seoul National University, Seoul, Korea; <sup>3</sup>Center for Ionizing Radiation, Korea Research Institute of Standards and Sciences, Daejeon, Korea; and <sup>4</sup>Department of Biomedical Sciences, College of Medicine, Seoul National University, Seoul, Korea

---

Personalized dosimetry with high accuracy is becoming more important because of the growing interest in personalized medicine and targeted radionuclide therapy. Voxel-based dosimetry using dose point kernel or voxel S-value (VSV) convolution is available. However, these approaches do not consider the heterogeneity of the medium. Here, we propose a new method for whole-body voxel-based personalized dosimetry in heterogeneous media with nonuniform activity distributions—a method we refer to as the multiple VSV approach. Instead of using only a single VSV, as found in water, the method uses multiple numbers ( $N$ ) of VSVs to cover media of various density ranges, as found in the whole body. **Methods:** The VSVs were precalculated using GATE Monte Carlo simulation and were convoluted with the time-integrated activity to generate density-specific dose maps. CT-based segmentation was performed to generate a binary mask image for each density region. The final dose map was acquired by the summation of  $N$  segmented density-specific dose maps. We tested several sets of VSVs with different densities:  $N = 1$  (single water VSV), 4, 6, 8, 10, and 20. To validate the proposed method, phantom and patient studies were conducted and compared with the direct Monte Carlo approach, which was considered the ground truth. Finally, dosimetry on 10 patients was performed using the multiple VSV approach and compared with the single VSV and organ-based approaches. Errors at the voxel and organ levels were reported for 8 organs. **Results:** In the phantom and patient studies, the multiple VSV approach showed significant decreases in voxel-level errors, especially for the lung and bone regions. As the number of VSVs increased, voxel-level errors decreased, although some overestimations were observed at the lung boundaries. For the multiple VSVs ( $N = 8$ ), we achieved a voxel-level error of 2.06%. In the dosimetry study, our proposed method showed greatly improved results compared with single VSV and organ-based dosimetry. Errors at the organ level were  $-6.71\%$ ,  $2.17\%$ , and  $227.46\%$  for single VSV, multiple VSV, and organ-based dosimetry, respectively. **Conclusion:** The multiple VSV approach for heterogeneous media with

nonuniform activity distributions offers fast personalized dosimetry at the whole-body level, yielding results comparable to those of the direct Monte Carlo approach.

**Key Words:** radiation dosimetry; Monte Carlo simulation; voxel S value; heterogeneous medium

**J Nucl Med 2018; 59:1133–1139**

DOI: 10.2967/jnumed.117.201095

---

**D**osimetry in nuclear medicine, or internal dosimetry, is important for evaluating radiation dose distributions of therapeutic or diagnostic radiopharmaceuticals inside the body. Internal dosimetry has become more important in recent years because of the growing interest in personalized medicine and targeted radionuclide therapy (1). For risk–benefit assessment of radiopharmaceuticals in clinical applications, more accurate dosimetry techniques may be required.

Internal dosimetry is widely conducted using the method proposed by the MIRD committee of the Society of Nuclear Medicine and Molecular Imaging (2–4). Traditionally, the MIRD approach was an organ-based dosimetry technique and provided dose distributions for the general population, whereas the latest MIRD approach was recently applied to tissues at suborgan or even cellular levels (5). The organ-based MIRD dosimetry approach uses organ-level S-values, which represent mean absorbed doses to target organs per unit activity in source organs. The limitations of this approach are that it assumes a uniform distribution of activity in organs and does not consider patient-specific anatomy.

Hence, to consider the nonuniform activity distributions in organs, voxel-based dosimetry techniques have been suggested, including the dose point kernel (DPK) (6,7) and voxel S-value (VSV) approaches (8). The DPK is the radial absorbed dose distribution around an isotropic point source in a homogeneous water medium; it is the most widely used voxel-based dosimetry approach (9–13). The VSV is the voxel-level approach of the organ-based MIRD schema; sources and targets are defined as voxels, and the voxel-level S-value is calculated in the water medium. The VSV approach has an advantage over DPK in that there is no need for central processing unit (CPU)–intensive conversion of spheric coordinates to Cartesian coordinates over the target volumes (8).

---

Received Aug. 28, 2017; revision accepted Nov. 21, 2017.  
For correspondence or reprints contact either of the following:  
Jae Sung Lee, Department of Nuclear Medicine, Seoul National University College of Medicine, 103 Daehak-ro, Jongno-gu, Seoul 03080, Korea.  
E-mail: jaes@snu.ac.kr  
Joong Hyun Kim, Center for Ionizing Radiation, Korea Research Institute of Standards and Science, 267 Gajeong-ro, Yuseong-gu, Daejeon 34113, Korea.  
E-mail: kimjh14@kriss.re.kr  
Published online Dec. 14, 2017.  
COPYRIGHT © 2018 by the Society of Nuclear Medicine and Molecular Imaging.

However, the VSV approach requires tabulated S-values for each isotope with the corresponding voxel size. In the conventional single VSV approach, the voxel dose ( $D_{\text{voxel}}$ ) is calculated by convoluting the time-integrated activity ( $\tilde{A}$ ) with the water-medium-based  $\text{VSV}_{\text{water}}$  as shown below:

$$D_{\text{voxel}_j} = \tilde{A} \otimes \text{VSV}_{\text{water}} = \sum_{i=0}^n \tilde{A}_{\text{voxel}_i} \times \text{VSV}_{\text{water}}(\text{voxel}_j \leftarrow \text{voxel}_i).$$

Eq. 1

However, the medium heterogeneities are not considered in either the DPK or the VSV approach; thus, in general, applicable cases are limited to lesions in homogeneous tissue media such as liver cancer. Previous studies noted the errors in dose calculations when using DPK methods without considering medium heterogeneities (14,15).

The direct Monte Carlo approach is a voxel-based dosimetry technique that accounts for heterogeneous activities and medium distributions. Up to now, the direct Monte Carlo approach, which tracks particles generated by Monte Carlo engines and calculates deposited energies at the voxel level, can provide an accurate dosimetric estimate depending on the accuracy of the applied models (16,17). However, the direct Monte Carlo approach requires extensive computational resources and time.

In this study, we propose a fast and new voxel-based dosimetry that can be applied not only to heterogeneous activities but also to heterogeneous media. The proposal is to use multiple VSVs to cover media of various density ranges, as found in the whole body. Multiple VSVs of various densities acquired from Monte Carlo simulation are used to create dose maps with CT-based segmentation. For validation, the multiple VSV approach was used on a digital phantom and whole-body PET images and compared with the direct Monte Carlo approach. Finally, we performed whole-body dosimetry studies using dynamic patient data and compared the proposed approach with the organ-based and direct Monte Carlo approaches.

## MATERIALS AND METHODS

### Subjects and PET/CT Procedure

This study retrospectively used the patient datasets (4 female and 6 male subjects) acquired in one of our previous studies (18). Dynamic PET/CT images were acquired after an intravenous injection of  $^{68}\text{Ga}$ -NOTA-RGD. The detailed imaging protocol was described by Kim et al. (18). The Institutional Review Board of Seoul National University Hospital approved the study, and all subjects gave written informed consent. Three-dimensional (3D) regions of interest for 8 organs—gallbladder, heart, kidneys, liver, lungs, pancreas, spleen, and stomach—were manually drawn on CT images.

### Direct Monte Carlo Approach: Setup for GATE Monte Carlo Simulation

The Geant4 Application for Emission Tomography (GATE) v.7.0 Monte Carlo simulation toolkit was used for the direct Monte Carlo approach and VSV precalculation (19,20). Many previous publications have already validated the dosimetric accuracy of the GATE toolkit (20–22). The standard electromagnetic physics package of Geant4 v.9.6.3 (23) was used to simulate particle and photon interactions. Acquired CT and PET images were modified to have the same matrix and pixel size and were used as the input. CT images were used to simulate the voxelized phantom, and Hounsfield units were converted into a 3D density map with corresponding elemental compositions

based on a previously published database (24). PET images were used to simulate voxelized  $^{68}\text{Ga}$  source distributions. The “DoseActor” mechanism in GATE was used for dose calculation (20).

The simulation was conducted using an in-house computing cluster with a 60-core CPU and 80 GB of random-access memory. Because of the long simulation time and extensive computational cost of the complete simulation, the simulation was performed for 5% of the scan duration while guaranteeing statistical uncertainties of 0.1% at the voxel level. The direct Monte Carlo approach using the GATE toolkit was considered the ground truth.

### Multiple VSV Approach

In the first step of the multiple VSV approach, VSVs of various densities and elemental compositions were precalculated with the GATE toolkit (Table 1 and Supplemental Table 1; supplemental materials are available at <http://jnm.snmjournals.org>). The  $^{68}\text{Ga}$  point source was located at the center voxel, and  $10^8$  primary particles were generated. The voxel size was  $2.67 \times 2.67 \times 5 \text{ mm}^3$ , which was the same as the PET pixel size. The VSV kernel size was set to  $101 \times 101 \times 51$ . The kernel size was determined to sufficiently cover the dose range to avoid underestimation of the absorbed dose, because  $^{68}\text{Ga}$  is a diagnostic radioisotope (25).

Second, density-specific dose maps,  $D_k$  (where  $k = 1, \dots, N$ , and  $N$  is the number of VSVs of different density ranges used) (mGy), were estimated by convoluting the PET time-integrated activity map,  $\tilde{A}$  (MBq·s), with each  $N$   $\text{VSV}_k$  (mGy/MBq·s). Figure 1, step 2 shows an example in which  $N$  is 4. The basic assumption here is that most organ energy depositions arise from self-absorption.

Third, CT-based segmentation was performed. For each density range, binary mask ( $\text{BM}_k$ ) images ( $\text{BM}_k = 1: d_k \leq d \leq d_{k+1}$ ;  $\text{BM}_k = 0$ : otherwise) were generated as in Figure 1, step 3. Consequently, each density-specific  $N$  dose map was multiplied by the corresponding binary

**TABLE 1**  
Densities of Simulated Multiple VSVs

Medium	Density (g/cm <sup>3</sup> )
Air	0.00129
Medium 1	0.1
Lung	0.26
Medium 2	0.3
Medium 3	0.4
Medium 4	0.5
Medium 5	0.6
Medium 6	0.7
Medium 7	0.8
Medium 8	0.9
Water	1.0
Medium 9	1.1
Medium 10	1.2
Medium 11	1.3
Bone	1.42
Medium 12	1.5
Medium 13	1.6
Medium 14	1.7
Medium 15	1.8
Medium 16	1.9

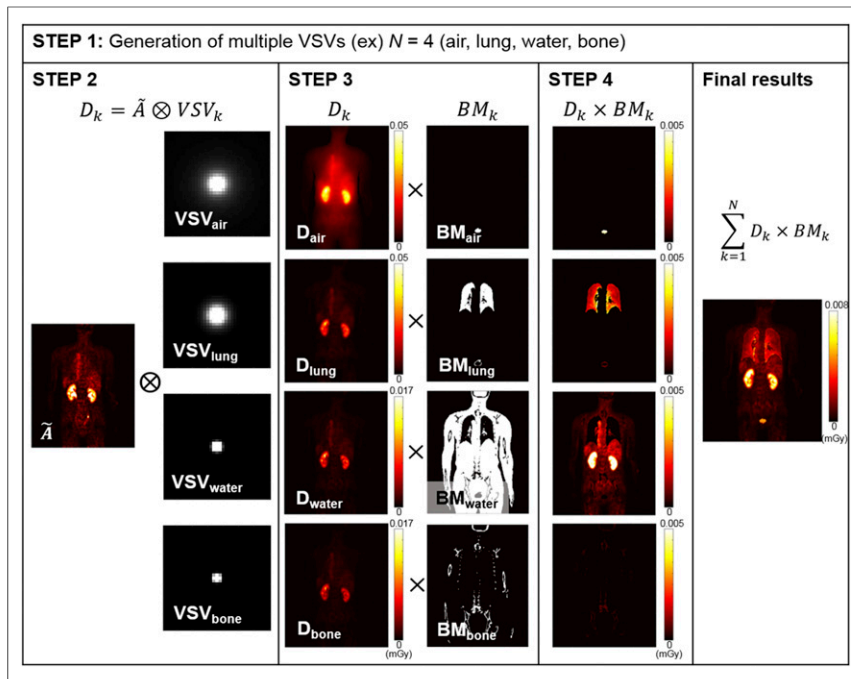


**FIGURE 1.** Multiple VSV approach with  $N = 4$ . VSVs of different densities were precalculated using GATE simulation (step 1). Density-specific dose maps were acquired by convoluting PET time-integrated activity maps with corresponding VSVs (step 2). Each density-specific dose map was segmented into corresponding density regions using CT-based binary mask images (step 3). Final dose map was acquired by summing segmented density-specific dose maps (step 4).

mask image, and the final 3D dose map ( $D$ ) was generated by summation as in Equation 2.

$$D = \sum_{k=1}^N D_k \times BM_k = \sum_{k=1}^N (\tilde{A} \otimes VSV_k) \times BM_k. \quad \text{Eq. 2}$$

By increasing the number of VSVs, we expect to reduce errors in dose estimation by reducing the number of mismatched media. We tested the proposed approach while changing the number of incorporated VSVs ( $N$ ):  $N = 1$  (conventional water-based VSV approach, single VSV), 4, 6, 8, 10, and 20. Tables 1 and 2 summarize the media and densities for each set of VSVs. For the  $N = 1$  case, single VSV approach, the medium was water. For the  $N = 4$  case, the simplest case of the multiple VSV approaches, air, lung, water, and bone were selected as the 4 media. For the  $N = 6$  case, fat ( $d = 0.9 \text{ g/cm}^3$ ) and bone marrow ( $d = 1.2 \text{ g/cm}^3$ ) were included, and for the  $N = 8$  case, dense lung ( $d = 0.4 \text{ g/cm}^3$ )

**TABLE 2**  
Media Used in the Various Sets of VSVs

No. of VSVs	Media
1	Water
4	Air, lung, water, bone
6	Air, lung, water, bone, medium 8, medium 10
8	Air, lung, water, bone, medium 3, medium 8, medium 10, medium 13
10	Air, lung, water, bone, medium 3, medium 5, medium 8, medium 10, medium 13, medium 15
20	All

and dense bone ( $d = 1.6 \text{ g/cm}^3$ ) were included. Further materials were involved for  $N = 10$  and 20 as detailed in Table 2.

### Implementation of the Proposed Method: Phantom and Patient Studies

As a validation step, the multiple VSV approach was implemented on the digital phantom and real patient images. The 3D digital phantom was simulated as in Figure 2A using the GATE toolkit with 3 different media (lung, water, and bone) with the unit activity distribution. Multiple VSV ( $N = 4$ ) and single VSV ( $N = 1$ ) approaches were implemented and compared with the ground truth.

Moreover, the multiple VSV approach with different numbers ( $N$ ) of VSVs was implemented on 80 patient PET datasets and compared with the direct Monte Carlo approach to evaluate dosimetric accuracy on more sophisticated medium distributions. Errors at the voxel level are reported as absolute and relative differences for 8 organs and represented as 3D difference maps over the whole body.

### Whole-Body Patient Dosimetry Study

Finally, whole-body dosimetry studies were performed using the multiple VSV approach and compared with direct Monte Carlo and organ-based dosimetry using OLINDA/EXM software

(4). Ten dynamic patient PET/CT datasets were used to conduct dosimetry studies. Dose maps were acquired at each time point using different dosimetry approaches, and time-integrated energy depositions per voxel were calculated by multiplying time-integrated dose by voxel mass. Absorbed doses for each organ were calculated by summing time-integrated energy deposition within the regions of interest and subsequently dividing by the organ masses of the Oak Ridge National Laboratory stylized phantoms for a fair comparison with organ-based dosimetry (4). The organ-based dosimetry results were previously published by Kim et al. (18).

## RESULTS

### Phantom Study

Dose profiles were generated from the phantom as shown in Figure 2B. The multiple VSV approach with  $N = 4$  agreed well with the direct Monte Carlo approach for lung, water, and bone media, whereas the single VSV approach ( $N = 1$ ) agreed only for water. However, we observed a slightly false estimation at the lung-to-water boundary. The error occurred because we

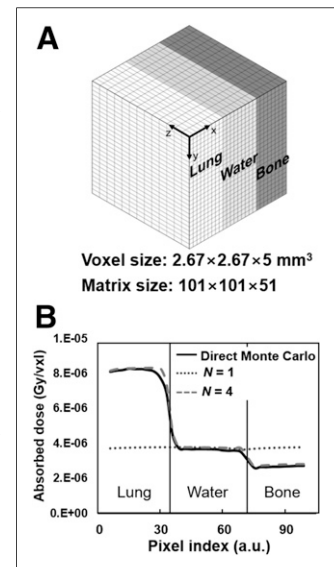


**FIGURE 2.** (A) Simulated digital phantom anatomy. (B) Results of phantom study. Absorbed dose profiles along lung, water, and bone media were calculated by direct Monte Carlo, single VSV, and 4-VSV approaches. a.u. = arbitrary units.

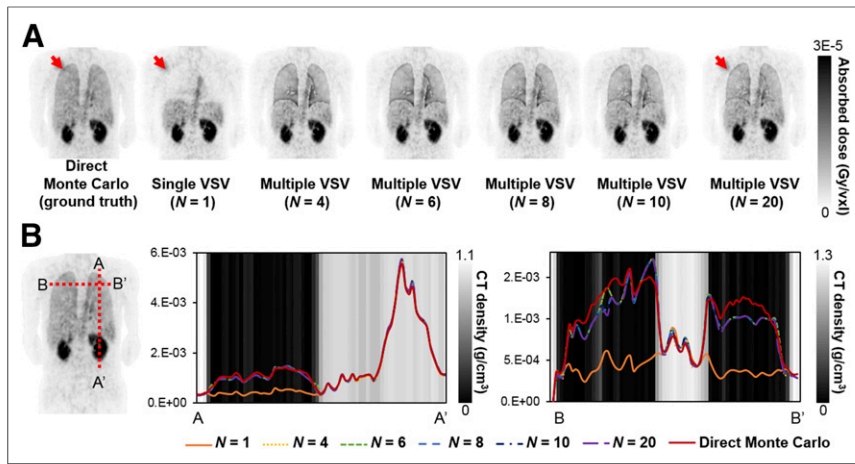


**FIGURE 3.** (A) Dose maps acquired using direct Monte Carlo, single VSV ( $N = 1$ ), and multiple VSV approaches ( $N = 4, 6, 8, 10$ , and  $20$ ). (B) Two dose profiles drawn on coronal slices.

performed VSV kernel convolution over the whole body, supposing that the total body is comprised of media of the same densities as shown in step 1 of Figure 1, on the assumption that most organ doses are contributed from self-absorption. Hence, for low-density media such as lungs, doses will be overestimated because the amount of self-absorption decreases, and this situation is especially noticeable at the lung boundaries. However, this false estimation was observed within only 1–2 voxels ( $\sim 4$  mm).

#### Patient Study

The multiple VSV approach was performed with different numbers of VSVs ( $N = 4, 6, 8, 10$ , and  $20$ ) on 80 static patient PET/CT

images and compared with the direct Monte Carlo and single VSV approaches. The representative coronal dose maps of 1 patient in Figure 3A clearly show that dose estimation at the lung regions improved dramatically with the multiple VSV approach. When the number of VSVs ( $N$ ) was increased, the dose maps better resembled the ground truth, especially at the lung boundaries. Figure 3B shows the dose profiles for each method along the left-lung/liver/kidney border and the left-lung/bone/right-lung border, with the background black-and-white images representing the corresponding medium densities along the profiles. In the soft-tissue regions, all VSV approaches showed similar results and matched the direct Monte Carlo approach well. In the lung regions, the single VSV approach

resulted in great underestimation, whereas the multiple VSV approach was better.

To quantitatively evaluate the accuracy of our proposed method, we calculated relative and absolute differences at the voxel level. They are presented as 3D maps in Figure 4 and Supplemental Figure 1, and relative differences are reported in Supplemental Table 2. In Figure 4, our proposed method shows prominently better results than the single VSV approach. For multiple VSV approaches with  $N > 6$ , difference maps showed enhanced results at the patient whole-body level, with large improvements at the lung boundaries and bones. Overestimation was observed at the lung boundaries, but this was decreased when larger numbers of VSVs were used. Furthermore, we observed underestimation in

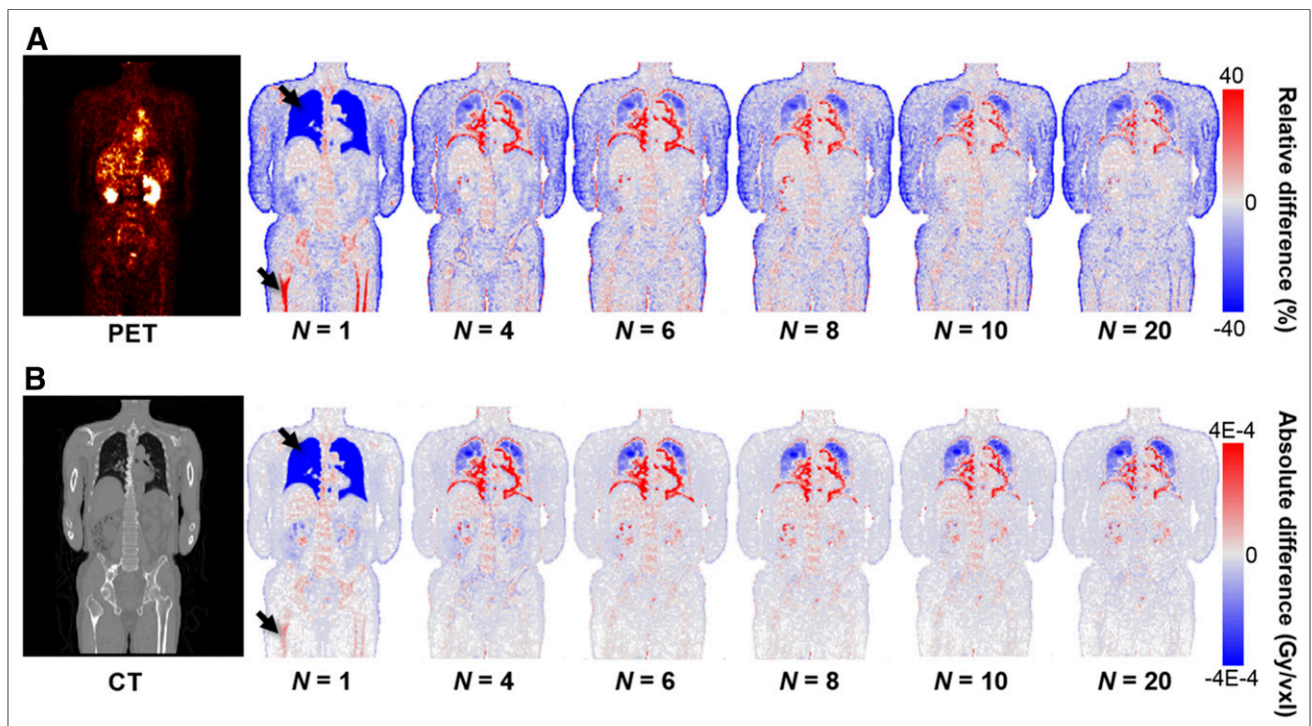


**FIGURE 4.** Errors at voxel level represented as relative (A) and absolute (B) differences. Difference maps were generated for single VSV and multiple VSVs ( $N = 4, 6, 8, 10$ , and  $20$ ).

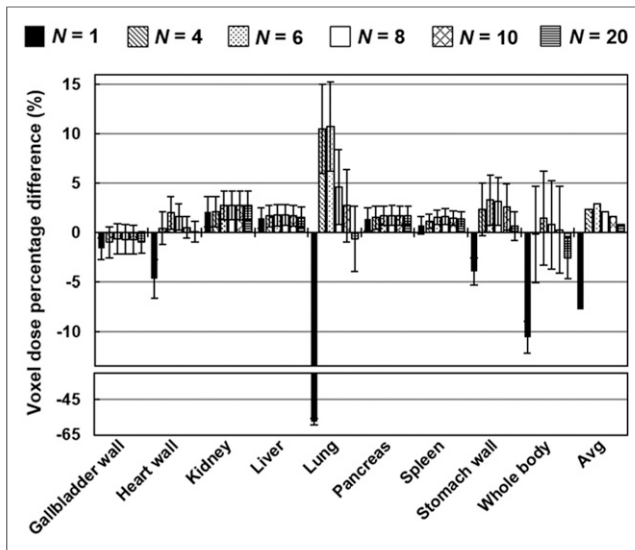


**FIGURE 5.** Plot of patient study results. Voxel dose percentage differences are reported for 8 different organs and whole body. Mean percentage differences of each method are indicated as boxes, and SDs are indicated as whiskers.

regions of low radioactivity because of statistical uncertainty. The air cavity regions showed the worst results.

From the difference maps, organ-level voxel dose errors were reported as relative differences for 8 organs and the whole body (Fig. 5). The multiple VSV approach showed results similar to but better than those of the single VSV approach for most organs and the whole body. The multiple VSV approach achieved a voxel dose percentage difference of under 5% for most organs. With multiple VSV ( $N = 20$ ), an average voxel dose percentage difference of 0.80% was achieved for the 8 organs.

#### Whole-Body Dosimetry in Patients

Our multiple VSV approach was successfully implemented and showed good results in both phantom and patient studies. Moreover, whole-body dosimetry using our proposed method was shown to be

feasible. As a final step, we performed whole-body patient dosimetry using the multiple VSV approach and compared it with direct Monte Carlo and organ-based dosimetry.

Table 3 summarizes the results for organ dose percentage difference averaged over 10 patients for all VSV approaches ( $N = 1, 4, 6, 8, 10, \text{ and } 20$ ), and the organ-based approach. Moreover, as representative results, organ dose percentage differences in the single VSV, the multiple VSV ( $N = 8$ ), and the organ-based results were compared (Fig. 6). Among the 3 methods, the multiple VSV approach using 8 VSVs showed the best results: errors at the organ level were  $-6.71\%$ ,  $2.17\%$ , and  $227.46\%$  on average for the single VSV, multiple VSV ( $N = 8$ ), and organ-based dosimetry results. Because the organ-based approach does not take into account personalized patient anatomies and heterogeneous activity distributions, we observed large differences and SDs for that approach. In particular, the pancreas showed the largest organ dose percentage difference, because the mass of the manually segmented pancreas differed most from the OLINDA/EXM phantom. By excluding the pancreas, we observed an average difference of  $16.07\%$ .

#### DISCUSSION

Voxel-based dosimetry has several advantages over conventional organ-based dosimetry. We can calculate dose information more accurately for an individual because voxel-based dosimetry uses real patient anatomies and activity distributions. In addition, because the dose information is given in the form of a 3D image, the whole-body dose distribution can be visualized more conveniently, and the dose-volume histograms for the targets can be assessed using heterogeneous dose information.

Several groups have suggested fast voxel-based dosimetry approaches based on the DPK or VSV. One approach is to use correction factors for heterogeneous tissues and media. Loudos et al. (26) suggested using medium-specific dose absorption factors derived from the water DPK and CT images. Voxel-based dose correction was applied using medium-specific dose absorption factors. Dieudonné et al. (27) performed voxel-level density correction for heterogeneous tissues in abdominal regions using a correction

**TABLE 3**  
Whole-Body Patient Dosimetry Results

Site	No. of VSVs						Organ-based approach
	1	4	6	8	10	20	
Gallbladder wall	-0.03	0.24	0.60	0.60	0.57	0.49	7.24
Heart wall	-3.96	-0.23	1.08	0.91	0.11	-0.24	38.54
Kidney	1.78	1.78	2.40	2.40	2.40	2.40	-3.86
Liver	1.41	1.58	1.65	1.69	1.63	1.45	-18.08
Lung	-52.85	16.28	16.72	7.64	4.29	0.53	23.43
Pancreas	1.08	1.18	1.37	1.37	1.36	1.35	1707.15
Spleen	1.50	1.76	2.05	2.14	2.01	1.94	25.07
Stomach wall	-2.60	-0.18	0.66	0.65	0.25	-0.29	40.16
Average	-6.71	-2.80	-3.32	2.17	1.58	0.95	227.46
Average (excluding Pancreas)	-7.82	3.03	3.60	2.29	1.61	0.90	16.07

Data are organ dose percentage difference  $\left( = \frac{\text{VSV approach} - \text{direct Monte Carlo}}{\text{direct Monte Carlo}} \times 100 [\%] \right)$ .

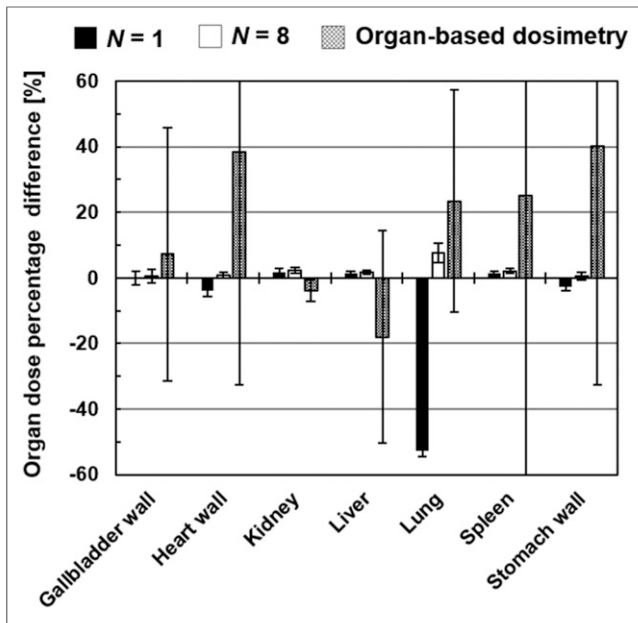


**FIGURE 6.** Whole-body dosimetry results for 10 patients. Organ dose percentage differences are reported for single VSV, multiple VSV ( $N = 8$ ), and organ-based dosimetry results.

factor consisting of the ratio of tissue density to voxel density. However, this approach has not been validated for highly heterogeneous regions. Another approach, recently suggested by Khazaei Moghadam et al. (28), applied tissue-specific DPKs, whereas the previous methods used only the water DPK. In the study of Khazaei Moghadam et al., DPKs for various media (such as bone, lung, adipose, and breast) were implemented in the mathematic Zubal phantom (29) and compared with the water DPK and direct Monte Carlo methods for several isotopes. The results showed improvement over the conventional water DPK method. However, that study was not performed on real patient data, which have highly complicated medium heterogeneities.

In this study, we developed a fast voxel-based dosimetry method that is applicable in heterogeneous media and at the whole-body

**TABLE 4**

Computation Time for 3D Dose Map Acquisition Using 4 CPU Cores and 16-GB Random-Access Memory

Method	Computation time (h)	Relative time
Direct Monte Carlo	235.20	1
Direct Monte Carlo (complete simulation)	4,704.03	20
Single VSV ( $N = 1$ )	0.17	0.00074
Multiple VSV ( $N = 4$ )	0.69	0.00295
Multiple VSV ( $N = 6$ )	1.04	0.00443
Multiple VSV ( $N = 8$ )	1.39	0.00591
Multiple VSV ( $N = 10$ )	1.74	0.00738
Multiple VSV ( $N = 20$ )	3.47	0.01476

level using multiple VSVs. The multiple VSV approach was implemented using 5 sets of different VSVs ( $N = 4, 6, 8, 10,$  and  $20$ ) on a digital phantom and real patient images and compared with the direct Monte Carlo approach to validate its dosimetric accuracy. As shown in Figures 3 and 4, our proposed method agreed well with the direct Monte Carlo approach. The multiple VSV approach had significantly better results than the single VSV approach, especially for organs—such as lungs and bones—that are more dense or less dense than tissues. When the number of VSVs was increased, errors at the voxel level decreased overall (Fig. 4). When the number of VSVs was larger than 6, the voxel-level errors were similar. Use of multiple VSVs with  $N = 20$  showed the best average voxel dose percentage difference, 0.80%, in organ evaluations.

Some false estimates were observed at the lung boundaries. In our proposed method, the basic assumption was that most organ doses are contributed from self-absorption, and hence the boundaries in organs of low density, such as the lung, were overestimated. However, this false estimation in lung boundaries existed for only 1–2 voxels. Moreover, lung regions have large motion artifacts, and because our interest in lung dosimetry is mainly tumors located inside organs, false estimation at the lung boundaries may not be a significant problem.

Finally, we performed whole-body dosimetry using the multiple VSV approach and compared it with single VSV, direct Monte Carlo, and organ-based dosimetry. We showed that the multiple VSV approach realizes personalized dosimetry at the whole-body level with high accuracy. Compared with the ground truth, the multiple VSV approach with  $N = 8$  showed an error of 2.17% at the organ level. When we used multiple VSV with  $N = 20$ , the results were comparable to those of the direct Monte Carlo approach. Organ-based dosimetry showed large errors, indicating that it is not adequate for personalized dosimetry.

Despite all the advantages of the direct Monte Carlo approach, it suffers in that it requires extensive computation resources. Our proposed method required significantly less computation time. Table 4 shows the computation time required to acquire a single dose map while using 4 CPU cores and 16 GB of random-access memory. Even when we used multicore CPUs to reduce the simulation time, the direct Monte Carlo approach took 235.2 h to generate a single dose map. By comparison, the multiple VSV with  $N = 8$  took a much shorter time, 1.39 h, for VSV precalculation and VSV kernel convolution with the PET time-integrated activity map. Therefore, using the multiple VSV approach, we can conduct fast dosimetry and visualize dose maps at the whole-body level with good dosimetric accuracy. The proposed method will be helpful in personalized medicine and targeted radionuclide therapy. Further studies are required to find the proper VSV kernel size depending on the emission type and the energies of the various radionuclides.

## CONCLUSION

In this paper, we have proposed a new voxel-based dosimetry approach using multiple VSVs that is applicable to heterogeneous media. Our proposed multiple VSV approach was successfully implemented in a patient dosimetry study and showed results comparable to those of the direct Monte Carlo approach, with the advantage of dramatically reduced dose calculation time.

## DISCLOSURE

This work was supported by the National Research Foundation of Korea (NRF), funded by the Korean Ministry of Science,

ICT, and Future Planning (grants NRF-2014M3C7034000 and NRF-2016R1A2B3014645). The funding source was not involved in study design, data collection, data analysis, or interpretation. No other potential conflict of interest relevant to this article was reported.

## REFERENCES

1. Fahey F, Zukotynski K, Capala J, et al. Targeted radionuclide therapy: proceedings of a joint workshop hosted by the National Cancer Institute and the Society of Nuclear Medicine and Molecular Imaging. *J Nucl Med.* 2014;55:337–348.
2. Berger MJ. Energy deposition in water by photons from point isotropic sources. *J Nucl Med.* 1968;2(suppl 1):17–25.
3. Loevinger R, Budinger TF, Watson EE. *MIRD Primer for Absorbed Dose Calculations.* Reston, VA: Society of Nuclear Medicine and Molecular Imaging; 1991.
4. Stabin MG, Sparks RB, Crowe E. OLINDA/EXM: the second-generation personal computer software for internal dose assessment in nuclear medicine. *J Nucl Med.* 2005;46:1023–1027.
5. Bolch WE, Eckerman KF, Sgouros G, Thomas SR. MIRD pamphlet no. 21: a generalized schema for radiopharmaceutical dosimetry—standardization of nomenclature. *J Nucl Med.* 2009;50:477–484.
6. Berger MJ. Distribution of absorbed dose around point sources of electrons and beta particles in water and other media. *J Nucl Med.* 1971;3(suppl 5):5–23.
7. Seltzer SM. Electron-photon Monte Carlo calculations: the ETRAN code. *Appl Radiat Isot.* 1991;42:917–941.
8. Bolch WE, Bouchet LG, Robertson JS, et al. MIRD pamphlet no. 17: the dosimetry of nonuniform activity distributions—radionuclide S values at the voxel level. *J Nucl Med.* 1999;40(suppl):11S–36S.
9. Kolbert KS, Sgouros G, Scott AM, et al. Implementation and evaluation of patient-specific three-dimensional internal dosimetry. *J Nucl Med.* 1997;38:301–308.
10. Campbell AM, Bailey IH, Burton MA. Tumour dosimetry in human liver following hepatic yttrium-90 microsphere therapy. *Phys Med Biol.* 2001;46:487–498.
11. Sgouros G, Barest G, Thekkumthala J, et al. Treatment planning for internal radionuclide therapy: three-dimensional dosimetry for nonuniformly distributed radionuclides. *J Nucl Med.* 1990;31:1884–1891.
12. Giap HB, Macey DJ, Bayouth JE, Boyer AL. Validation of a dose-point kernel convolution technique for internal dosimetry. *Phys Med Biol.* 1995;40:365–381.
13. Sgouros G, Kolbert KS, Sheikh A, et al. Patient-specific dosimetry for <sup>131</sup>I thyroid cancer therapy using <sup>124</sup>I PET and 3-dimensional-internal dosimetry (3D-ID) software. *J Nucl Med.* 2004;45:1366–1372.
14. Cristy M. Applying the reciprocal dose principle to heterogeneous phantoms: practical experience from Monte Carlo studies. *Phys Med Biol.* 1983;28:1289–1303.
15. Kwok CS, Bialobzyski PJ, Yu SK, Prestwich WV. Effect of tissue inhomogeneity on dose distribution of point sources of low-energy electrons. *Med Phys.* 1990;17:786–793.
16. Furhang EE, Chui CS, Sgouros G. A Monte Carlo approach to patient-specific dosimetry. *Med Phys.* 1996;23:1523–1529.
17. Zaidi H. Relevance of accurate Monte Carlo modeling in nuclear medical imaging. *Med Phys.* 1999;26:574–608.
18. Kim JH, Lee JS, Kang KW, et al. Whole-body distribution and radiation dosimetry of <sup>68</sup>Ga-NOTA-RGD, a positron emission tomography agent for angiogenesis imaging. *Cancer Biother Radiopharm.* 2012;27:65–71.
19. Jan S, Santin G, Strul D, et al. GATE: a simulation toolkit for PET and SPECT. *Phys Med Biol.* 2004;49:4543–4561.
20. Sarrut D, Bardies M, Bousson N, et al. A review of the use and potential of the GATE Monte Carlo simulation code for radiation therapy and dosimetry applications. *Med Phys.* 2014;41:064301.
21. Papadimitroulas P, Loudos G, Nikiforidis GC, Kagadis GC. A dose point kernel database using GATE Monte Carlo simulation toolkit for nuclear medicine applications: comparison with other Monte Carlo codes. *Med Phys.* 2012;39:5238–5247.
22. Maigne L, Perrot Y, Schaart DR, Donnarieix D, Breton V. Comparison of GATE/GEANT4 with EGSnrc and MCNP for electron dose calculations at energies between 15 keV and 20 MeV. *Phys Med Biol.* 2011;56:811–827.
23. Agostinelli S, Allison J, Amako K, et al. GEANT4: a simulation toolkit. *Nucl Instrum Methods Phys Res A.* 2003;506:250–303.
24. Schneider W, Bortfeld T, Schlegel W. Correlation between CT numbers and tissue parameters needed for Monte Carlo simulations of clinical dose distributions. *Phys Med Biol.* 2000;45:459–478.
25. Marcatili S, Villoing D, Mauxion T, McParland BJ, Bardies M. Model-based versus specific dosimetry in diagnostic context: comparison of three dosimetric approaches. *Med Phys.* 2015;42:1288–1296.
26. Loudos G, Tsougos I, Boukis S, et al. A radionuclide dosimetry toolkit based on material-specific Monte Carlo dose kernels. *Nucl Med Commun.* 2009;30:504–512.
27. Dieudonné A, Hobbs RF, Lebtani R, et al. Study of the impact of tissue density heterogeneities on 3-dimensional abdominal dosimetry: comparison between dose kernel convolution and direct Monte Carlo methods. *J Nucl Med.* 2013;54:236–243.
28. Khazaei Moghadam M, Asl AK, Geramifar P, Zaidi H. Evaluating the application of tissue-specific dose kernels instead of water dose kernels in internal dosimetry: a Monte Carlo study. *Cancer Biother Radiopharm.* 2016;31:367–379.
29. Zubal IG, Harrell CR, Smith EO, Rattner Z, Gindi G, Hoffer PB. Computerized three-dimensional segmented human anatomy. *Med Phys.* 1994;21:299–302.